Stiffness modeling of NAVARO II transmission system

A. Klimchik, Anatol Pashkevich, Damien Chablat

Stiffness modeling of NAVARO II transmission system

A. Klimchik[*], A. Pashkevich[*,], D. Chablat[***]**

*Innopolis University, Universitetskaya 1, 420500 Innopolis, The Republic of Tatarstan, Russia
(e-mail: a.klimchik@innopolis.ru)
** IMT Atlantique, 4 rue Alfred-Kastler, Nantes 44307, Le Laboratoire des Sciences du Numérique de Nantes (LS2N)
(e-mail: anatol.pashkevich@imt-atlantique.fr)
*** CNRS, Nantes, France, Le Laboratoire des Sciences du Numérique de Nantes (LS2N)
(e-mail: damien.chablat@cnrs.fr)

Abstract: The paper deals with stiffness modeling of NAVARO II transmission system, which is a novel variable actuation mechanism based on active and passive pantographs. The desired models are obtained using the enhanced matrix structural analysis (MSA) approach that is able to analyze the under-actuated and over-constrained structures with numerous passive joints. Depending on the pantograph type, the models operate with the matrices of size 252x288 and 264x294 suitable for parametric optimization of the entire manipulator.

Keywords: parallel robots, variable actuation transmission, stiffness analysis, MSA technique

1. INTRODUCTION

For most industrial robots, the actuator transmission system is one of the principal components defining the stiffness properties of an entire manipulator. For conventional serial manipulators, the elasticity of the transmission can be easily taken into account by introducing equivalent one-dimensional springs in actuated joints (Alici and Shirinzadeh, 2005, Klimchik and Pashkevich, 2017, Klimchik et al., 2017b, Klimchik et al., 2017a). A similar approach is also used for many parallel manipulators (GS platform, etc.) (Gosselin, 1990), where the actuator elasticity is modeled by one-dimensional springs integrated into the legs connected moving platform and the base. However, recent developments in parallel robotics produced new architectures for which traditional approach operating with one-dimensional equivalent springs can be hardly applied. In such manipulators, the moving platform is actuated via multi-link chains whose elasticity is multi-dimensional and configuration-dependent. This paper presents a stiffness analysis of one of such systems used in parallel manipulator NAVARO II and gives a general framework for elastostatic modeling of similar robots.

At present, there exist three main techniques for the stiffness modelling (Pashkevich et al., 2011b), which are the Finite Element Analysis (FEA) (Yan et al., 2016, Wang et al., 2006, Klimchik et al., 2013), the Matrix Structural Analysis (MSA) (Nagai and Liu, 2008, Marie et al., 2013, Deblaise et al., 2006) and the Virtual Joint Modelling (VJM) (Klimchik et al., 2012, Quennouelle and Gosselin, 2008, Gosselin and Zhang, 2002, Pashkevich et al., 2011a). The most accurate but computationally expansive is the FEA (Yan et al., 2016), while the MSA used in this paper is considered as a compromise technique since it operates with rather large flexible elements connected by the actuated and passive (Klimchik et al., 2019b).

The NAVARO II robot, whose transmission system is studied here, is a novel variable actuation mechanism based on modified 3-RPR parallel kinematics where the second revolute joint of each leg is replaced by a scissor (Chablat and Rolland, 2018). Such modification gives a number of benefits and allows excluding kinematic parallelograms that are traditionally used in similar manipulators. To obtain better spatial rigidity, the leg mechanism is constructed by placing the scissors in an orthogonal plane to the displacement.

The actuation system of NAVARO II can be considered as a double clutch and contains an electric motor and two electromechanical clutches connecting the motor shaft either to the first revolute joint or to the shaft of the prismatic joint. Two position sensors give the leg angular position relative to the base and the current length of the prismatic joint. Depending on the clutches' state, such kinematics allows to implement four actuation schemes where: (#0) the leg is not controlled and may freely change its length and orientation; (#1) the leg length may be arbitrary but its orientation is controlled; (#2) the leg length is controlled while its orientation may be arbitrary; (#3) both the leg length and orientation are controlled in order to execute synchronized translation/rotation. However, only the first and second schemes are studied in this paper because of their practical significance. It is clear that actuation scheme #0 is passive and cannot be used to control the mobile platform location.

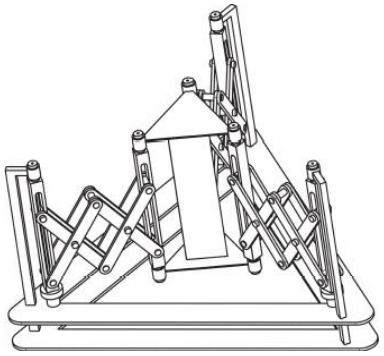

Figure 1. Parallel planar manipulator NaVaRo.

2. FUNDAMENTALS OF MSA MODELLING FOR ROBOTIC MANIPULATORS

For the stiffness modeling of NAVARO II manipulator, which includes numerous closed-loops and passive connections, it is reasonable to use the MSA-based technique. Main theoretical results in this area suitable for the analysis of under-constrained, fully actuated and over-constrained serial and parallel manipulators were presented in our previous works (Klimchik et al., 2018, Klimchik et al., 2019a, Klimchik et al., 2019b). Here, let us present a summary of this approach that will be further applied to the stiffness analysis of the NAVARO II parallel manipulator.

2.1. Modeling of manipulator links and platform

In the frame of the MSA technique, the manipulator is presented as a set of nodes connected by flexible or rigid links. The flexible link is described by the following linear matrix equation relating displacements at the end-nodes

$$\begin{bmatrix} \mathbf{W}_i \\ \mathbf{W}_j \end{bmatrix} = \begin{bmatrix} \mathbf{K}_{11}^{(ij)} & \mathbf{K}_{12}^{(ij)} \\ \mathbf{K}_{21}^{(ij)} & \mathbf{K}_{22}^{(ij)} \end{bmatrix}_{12\times12} \cdot \begin{bmatrix} \Delta\mathbf{t}_i \\ \Delta\mathbf{t}_j \end{bmatrix} \tag{1}$$

where $\Delta\mathbf{t}_i, \Delta\mathbf{t}_j$ are the deflections at the link ends, $\mathbf{W}_i, \mathbf{W}_j$ are the link end wrenches, i and j are the node indices, and $\mathbf{K}_{11}^{(ij)}$, $\mathbf{K}_{12}^{(ij)}$, $\mathbf{K}_{21}^{(ij)}$, $\mathbf{K}_{22}^{(ij)}$ are 6×6 stiffness matrices.

The moving platform is being presented as a set of elastic links connecting the nodes $i, j, k, ...$ of the manipulator leg clamping and the reference point node e. For the platform with three legs, this gives the following equation

$$\begin{bmatrix} \mathbf{W}_i \\ \mathbf{W}_j \\ \mathbf{W}_k \\ \mathbf{W}_e \end{bmatrix} = \begin{bmatrix} \mathbf{K}_{11}^{(ie)} & \mathbf{0}_{6\times6} & \mathbf{0}_{6\times6} & \mathbf{K}_{12}^{(ie)} \\ \mathbf{0}_{6\times6} & \mathbf{K}_{11}^{(je)} & \mathbf{0}_{6\times6} & \mathbf{K}_{12}^{(je)} \\ \mathbf{0}_{6\times6} & \mathbf{0}_{6\times6} & \mathbf{K}_{11}^{(ke)} & \mathbf{K}_{12}^{(ke)} \\ \mathbf{K}_{21}^{(ie)} & \mathbf{K}_{21}^{(je)} & \mathbf{K}_{21}^{(ke)} & \mathbf{K}_{22}^{(ie)} + \mathbf{K}_{22}^{(je)} + \mathbf{K}_{22}^{(ke)} \end{bmatrix} \cdot \begin{bmatrix} \Delta\mathbf{t}_i \\ \Delta\mathbf{t}_j \\ \Delta\mathbf{t}_k \\ \Delta\mathbf{t}_e \end{bmatrix} \tag{2}$$

where $\Delta\mathbf{t}_i, \Delta\mathbf{t}_j, \Delta\mathbf{t}_k$ are the deflections at the leg clamping points, $\Delta\mathbf{t}_e$ is the deflection at the end-effector reference point, $\mathbf{W}_i, \mathbf{W}_j$ $\mathbf{W}_k$ are the wrenches at the leg clamping points, $\mathbf{W}_e$ is the total wrench applied to the end-effector.

It should be mentioned that all stiffness matrices in eqs. (1) and (2) should be presented in a global coordinate system. Relevant numerical values of the stiffness matrix elements can be obtained either from the approximation of the links by regular beams or from the FEA-based experiments in the virtual environment using link's CAD models (Klimchik et al., 2013).

If the link flexibility is negligible, the stiffness model (1) should be replaced by the "rigidity constraint"

$$\begin{bmatrix} \mathbf{D}^{(ij)} & -\mathbf{I}_{6\times6} \end{bmatrix} \cdot \begin{bmatrix} \Delta\mathbf{t}_i \\ \Delta\mathbf{t}_j \end{bmatrix} = \mathbf{0}_{6\times1} \tag{3}$$

which includes 6×6 identity matrix $\mathbf{I}_{6\times6}$ and 6×6 matrix

$$\mathbf{D}^{(ij)} = \begin{bmatrix} \mathbf{I}_{3\times3} & [\mathbf{d}^{(ij)}\times]^T \\ \mathbf{0}_{3\times3} & \mathbf{I}_{3\times3} \end{bmatrix}_{6\times6} \tag{4}$$

where $[\mathbf{d}^{(ij)}\times]$ denotes the 3×3 skew-symmetric matrix derived from the vector $\mathbf{d}^{(ij)}$ describing link geometry.

In addition, it is necessary to take into account the force equilibrium that here can be presented in the following form

$$\begin{bmatrix} \mathbf{I}_{6\times6} & \mathbf{D}^{(ij)T} \end{bmatrix} \cdot \begin{bmatrix} \mathbf{W}_i \\ \mathbf{W}_j \end{bmatrix} = \mathbf{0}_{6\times1} \tag{5}$$

Totally, this yields 12 scalar equations describing relations between the displacements/wrenches, similarly to (1).

2.2. MSA models of manipulator's joints

To take into account connections between the adjacent links by means of joints, the stiffness model must include relations describing two principal rules of structural mechanics: (a) displacement compatibility, (b) force equilibrium. For the rigid joint, the displacement compatibility is expressed as

$$\begin{bmatrix} \mathbf{I}_{6\times6} & -\mathbf{I}_{6\times6} \end{bmatrix}_{6\times12} \cdot \begin{bmatrix} \Delta\mathbf{t}_i \\ \Delta\mathbf{t}_j \end{bmatrix} = \mathbf{0}_{6\times1} \tag{6}$$

and the force equilibrium is presented as

$$\begin{bmatrix} \mathbf{I}_{6\times6} & \mathbf{I}_{6\times6} \end{bmatrix}_{6\times12} \cdot \begin{bmatrix} \mathbf{W}_i \\ \mathbf{W}_j \end{bmatrix} = \mathbf{0}_{6\times1} \tag{7}$$

For the passive joint, the displacement compatibility condition contains only $r < 6$ equations

$$\begin{bmatrix} \mathbf{\Lambda}_{ij}^{r} & -\mathbf{\Lambda}_{*ij}^{r} \end{bmatrix}_{r\times12} \cdot \begin{bmatrix} \Delta\mathbf{t}_i \\ \Delta\mathbf{t}_j \end{bmatrix} = \mathbf{0}_{r\times1} \tag{8}$$

where $\mathbf{\Lambda}_{*}^{r} = \begin{bmatrix} \mathbf{u}_1, ..., \mathbf{u}_r \end{bmatrix}_{r\times6}^{T}$ is a rectangular matrix of the rank r that is formed the vectors $\mathbf{u}_1, \mathbf{u}_2, ..., \mathbf{u}_6$ composing the orthonormal basis associated with the orientation of passive joint(s) in such way that the unit vectors $\mathbf{u}_1, ..., \mathbf{u}_r$ describe the directions of the rigid connection and the unit vector(s) $\mathbf{u}_{r+1}, ..., \mathbf{u}_6$ correspond to the passive connection allowing free relative motions. In this case, the force equilibrium gives the following relations

$$\begin{bmatrix} \mathbf{\Lambda}_{*ij}^{r} & \mathbf{\Lambda}_{*ij}^{r} \\ \mathbf{\Lambda}_{*ij}^{p} & \mathbf{0} \\ \mathbf{0} & \mathbf{\Lambda}_{*ij}^{p} \end{bmatrix}_{(6+p)\times12} \cdot \begin{bmatrix} \mathbf{W}_i \\ \mathbf{W}_j \end{bmatrix} = \mathbf{0}_{(6+p)\times1} \tag{9}$$

where the matrix $\mathbf{\Lambda}_{*}^{p} = \begin{bmatrix} \mathbf{u}_{r+1}, ..., \mathbf{u}_6 \end{bmatrix}_{p\times6}^{T}$. It should be noted that all passive connections should be treated separately (in contrast to rigid ones).

For the elastic joint, the deflection compatibility condition (8) remains the same. However, the force equilibrium condition must be replaced by

$$\begin{bmatrix} \mathbf{0}_{6\times6} & \mathbf{0}_{6\times6} & \mathbf{I}_{6\times6} & \mathbf{I}_{6\times6} \\ \mathbf{K}_{ij}^{e}\mathbf{\Lambda}_{*ij}^{e} & -\mathbf{K}_{ij}^{e}\mathbf{\Lambda}_{*ij}^{e} & \mathbf{\Lambda}_{*ij}^{e} & \mathbf{0}_{e\times6} \end{bmatrix} \begin{bmatrix} \Delta\mathbf{t}_i \\ \Delta\mathbf{t}_j \\ \mathbf{W}_i \\ \mathbf{W}_j \end{bmatrix} = \begin{bmatrix} \mathbf{0}_{6\times1} \\ \mathbf{\Lambda}_{*ij}^{e}\mathbf{W}_{ij}^{0} \end{bmatrix} \tag{10}$$

where the matrix $\mathbf{\Lambda}_{*ij}^{e}$ of size $e\times6$, $e = 6-r$ corresponds to the non-rigid directions of the joint (similar to $\mathbf{\Lambda}_{*ij}^{p}$) and $\mathbf{K}_{ij}^{e}$ is $e\times e$ stiffness matrix describing elastic properties of the joint, $\mathbf{W}_{ij}^{0}$ is preloading in the corresponding springs.

2.3. Connection to the base and loadings

The rigid connection of the link to the robot base can be presented as a special case of the rigid joint with zero deflection $\Delta\mathbf{t}_j = \mathbf{0}$. This simplifies the deflection compatibility constraint (6) down to

$$\begin{bmatrix} \mathbf{I}_{6\times6} \end{bmatrix} \cdot \begin{bmatrix} \Delta\mathbf{t}_j \end{bmatrix} = \mathbf{0}_{6\times1} \tag{11}$$

The passive connection of the link to the robot base can be presented as a special case of the passive joint with zero deflection in the non-passive directions $\mathbf{\Lambda}^{r}_{*ij} \cdot \Delta\mathbf{t}_j = \mathbf{0}$. This reduces the deflection compatibility constraint (8) and force equilibrium to

$$\begin{aligned} &\left[\mathbf{\Lambda}^{r}_{*ij}\right]_{r\times 6} \cdot \left[\Delta\mathbf{t}_j\right] = \mathbf{0}_{r\times 1} \\ &\mathbf{\Lambda}^{p}_{*ij} \cdot \mathbf{W}_j = \mathbf{0}_{p\times 1} \end{aligned} \tag{12}$$

The elastic connection of the link to the robot base can be presented as a special case of the elastic joint with zero deflection in the non-elastic directions $\mathbf{\Lambda}^{r}_{*ij} \cdot \Delta\mathbf{t}_j = \mathbf{0}$. This allows us to use the following relation for deflection compatibility constraint and force equilibrium

$$\begin{aligned} &\left[\mathbf{\Lambda}^{r}_{*ij}\right]_{r\times 6} \cdot \left[\Delta\mathbf{t}_j\right] = \mathbf{0}_{r\times 1} \\ &\left[-\mathbf{K}^{e}_{ij} \cdot \mathbf{\Lambda}^{e}_{*ij} \;\vdots\; \mathbf{\Lambda}^{e}_{*ij}\right]_{e\times 12} \cdot \begin{bmatrix} \Delta\mathbf{t}_j \\ \mathbf{W}_j \end{bmatrix} = \left[\mathbf{\Lambda}^{e}_{*ij}\mathbf{W}^{0}_{ij}\right]_{e\times 1} \end{aligned} \tag{13}$$

To take into account the external loading $\mathbf{W}_e$, the global stiffness model must be extended by the linear equation ensuring the force equilibrium, i.e. $\mathbf{W}_i + \mathbf{W}_j + \mathbf{W}_k + \ldots = \mathbf{W}_e$, which can be rewritten in the form (for three adjacent links)

$$\left[\mathbf{I}_{6\times 6} \quad \mathbf{I}_{6\times 6} \quad \mathbf{I}_{6\times 6}\right]_{6\times 18} \cdot \begin{bmatrix} \mathbf{W}_i \\ \mathbf{W}_j \\ \mathbf{W}_k \end{bmatrix}_{18\times 1} = \left[\mathbf{W}_e\right]_{6\times 1} \tag{14}$$

A similar technique is used to all nodes where the external wrenches are applied.

4.4. Aggregation of MSA model components

After aggregation of all equation describing the manipulator links and their connections, the global stiffness model of the manipulator can be presented in the form

$$\begin{bmatrix} \mathbf{A}^{(1)}_{\mathrm{W}} & \mathbf{A}^{(1)}_{\Delta\mathrm{t}} \\ \mathbf{A}^{(2)}_{\mathrm{W}} & \mathbf{A}^{(2)}_{\Delta\mathrm{t}} \\ \cdots & \cdots \end{bmatrix} \cdot \begin{bmatrix} \{\mathbf{W}_i\} \\ \{\Delta\mathbf{t}_i\} \end{bmatrix} = \begin{bmatrix} \mathbf{b}^{(1)}_0 \\ \mathbf{b}^{(2)}_0 \\ \cdots \end{bmatrix} \tag{15}$$

where $\mathbf{W}_i$ and $\Delta\mathbf{t}_i$ are the wrench and displacement of the i^{th} node, the matrices $\mathbf{A}^{(i)}_{\mathrm{W}}$, $\mathbf{A}^{(i)}_{\Delta\mathrm{t}}$ and the vectors $\mathbf{b}^{(i)}_0$ are defined above using expressions presented in the previous sections. After rearranging the matrix rows and introducing relevant definitions for the blocks, the global stiffness model can be rewritten as

$$\left[\begin{array}{cc:c} \mathbf{S}_{agr} & \mathbf{K}_m & \mathbf{K}_e \\ \mathbf{E}_m & \mathbf{F}_m & \mathbf{C}_e \\ \hdashline \mathbf{E}_e & \mathbf{F}_e & \mathbf{D} \end{array}\right] \cdot \left[\begin{array}{c} \mathbf{W}_{agr} \\ \Delta\mathbf{t}_m \\ \hdashline \Delta\mathbf{t}_e \end{array}\right] = \left[\begin{array}{c} \mathbf{b}_{agr} \\ \mathbf{W}_m \\ \hdashline \mathbf{W}_e \end{array}\right] \tag{16}$$

where the matrices are obtained using relevant equations describing the links and connections, while the vectors $\mathbf{W}_{agr}$ and $\Delta\mathbf{t}_{agr} = [\Delta\mathbf{t}_m{}^T; \Delta\mathbf{t}_e{}^T]^T$ aggregate all variables describing the wrenches and displacements. The node displacement $\Delta\mathbf{t}_{agr}$ is divided into two groups $\Delta\mathbf{t}_m$ and $\Delta\mathbf{t}_e$ corresponding to the manipulator internal nodes and the end-effector node, where the external wrench $\mathbf{W}_e$ is applied. The latter allows us to obtain, the desired Cartesian stiffness matrix

$$\mathbf{K}_C = \mathbf{D} - \begin{bmatrix} \mathbf{E}_e & \mathbf{F}_e \end{bmatrix} \cdot \begin{bmatrix} \mathbf{S}_{agr} & \mathbf{K}_m \\ \mathbf{E}_m & \mathbf{F}_m \end{bmatrix}^{-1} \cdot \begin{bmatrix} \mathbf{K}_e \\ \mathbf{C}_e \end{bmatrix} \tag{17}$$

where the matrix inversion usually exists (if the manipulator does not include redundant passive joints).

3. NAVARO II MANIPULATOR ARCHITECTURE

3.1. Particularities of NAVARO II architecture

NAVARO II is a special case of the 3-RPR manipulator (Fig. 2) where the translational joint is implemented by means of double clutch pantograph-type transmission presented in Fig. 3. In more details, the architecture of this manipulator is presented in Fig. 1.

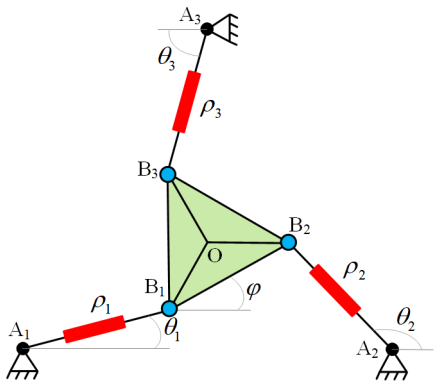

Figure 2. Kinematic model of NAVARO II manipulator.

Due to the double-clutch system, the transmission allows to implement three following actuation modes:

Mode #1: Clutch 1 is active while clutch 2 is passive. The first leg axis (green) is driven by the rotation of the motor shaft. In this case, the angle θ is active while ρ is passive.

Mode #2: Clutch 2 is active while clutch 1 is passive. The first leg joint is free, but the rotation of the motor shaft leads to a displacement of the slider, which activates the scissors. In this case, the θ is passive and ρ is active.

Mode #3: Both clutches 1 and 2 are active. Both joints cause a synchronized rotation and translation motion. The end of the leg will make a spiral motion.

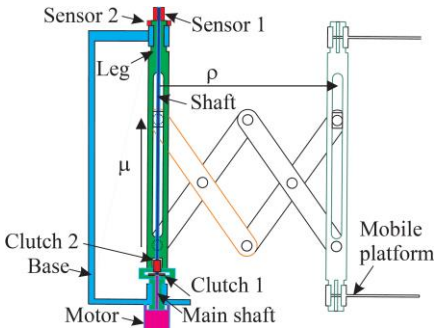

Figure 3. Kinematic model of NAVARO II transmission.

In this paper, we will focus on the stiffness analysis of the NAVARO II manipulator and its transmission for the actuation modes #1 and #2, which are the most interesting for practical application.

3.2. Kinematics of NAVARO II manipulator

To estimate the manipulator stiffness behavior within its workspace it is required to obtain relations allowing to find the transmission variables θ_i and ρ_i corresponding to the given end-effector location, i.e. to solve the inverse kinematic problem. For this manipulator, for any given end-effector

position $\mathbf{O}$ and platform orientation φ, the positions of the platform connection points $\mathbf{B}_i$ can be computed as

$$\mathbf{B}_i = \mathbf{O} - \mathbf{R}_z\left(-\frac{\pi}{6} + \frac{2\pi}{3}\cdot(i-2) + \varphi\right)\cdot\begin{bmatrix} r \\ 0 \\ 0 \end{bmatrix}, \qquad i = 1,2,3 \qquad (18)$$

where r is the distance from the platform center to the connection points (the same for all points), and $\mathbf{R}_z(.)$ is elementary rotation matrix around z-axis. This allows us to find the pantograph orientation θ_i and leg length ρ_i (pantograph length) for the known leg base positions $\mathbf{A}_i$ from the following equations

$$\begin{aligned} \theta_i &= \operatorname{atan2}(\mathbf{B}_{yi} - \mathbf{A}_{yi}, \mathbf{B}_{xi} - \mathbf{A}_{xi}) \\ \rho_i &= \|\mathbf{B}_i - \mathbf{A}_i\| \end{aligned}, \qquad i = 1,2,3 \qquad (19)$$

It should be noted that the inverse kinematic solution exists for reachable mobile platform location only, which is specified by minimum and maximum pantograph lengths, i.e.

$$\rho_{\min} \le \rho_i \le \rho_{\max} \qquad (20)$$

The values ρ_i will be used further to compute orientations of the pantograph internal links.

3.3. Kinematics of NAVARO II transmission system

As it was mentioned before, the NAVARO II controller may utilize two actuation mode (types of transmission): with active and passive pantographs (Fig. 4). Clearly, this effects on the transmission stiffness properties while from the kinematical point of view these cases are identical.

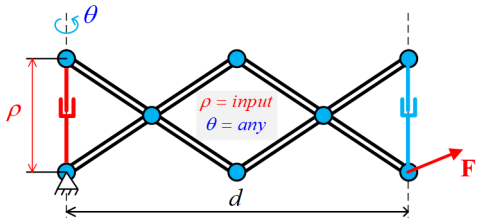

(a) Active pantograph

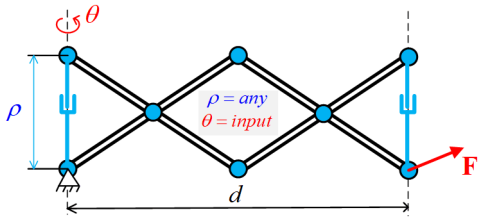

(b) Passive pantograph

Figure 4. Equivalent models of NAVARO II transmission.

For both passive and active pantographs, the inverse kinematics problem (giving the orientation of the transmission links) can be solved using the relation between the length of the leg ρ and the length of pantograph links l

$$2l\cos\beta = \rho \qquad (21)$$

That gives the following expressions for the links orientations

$$\beta_{up} = \operatorname{acos}(\rho/2l), \qquad \beta_{down} = \pi/2 - \beta_{up} \qquad (22)$$

The latter allows us to compute the orientation of each link of the pantograph transmission and to transform the link stiffness matrices into the global coordinate system.

4. MSA MODELS OF MANIPULATOR COMPONENTS

To apply the MSA technique for the stiffness modeling of NAVARO II, let us split the manipulator into four parts: three kinematically identical legs and the mobile platform, which is actuated by means of either passive or active pantographs. The MSA representations for these principal components are shown in Fig. 5. Relevant models are composed of a number of flexible and rigid links (i,j) connected in a special way by passive, rigid and elastic joints $<i,j>$. The model components are also listed in Table 1.

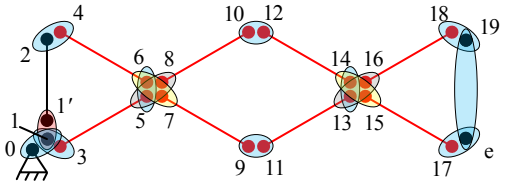

(a) Active pantograph

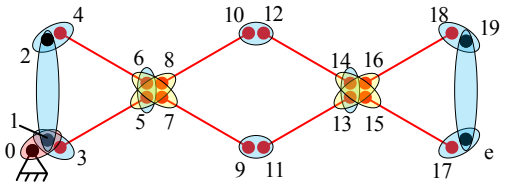

(b) Passive pantograph

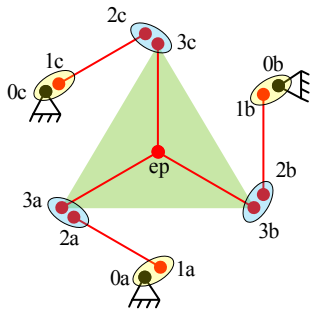

(c) Entire manipulator

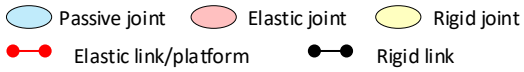

Figure 5. MSA-based representation of the NAVARO II manipulator.

4.1. MSA models of pantograph-type transmission system

In order to obtain stiffness model of entire NAVARO II mechanism let us first derive the stiffness model for separate legs represented via passive or active pantographs. AS follows from Figure 5a,b the leg is composed of a set of eight flexible links (3,5), (4,6), (7,9), (8,10), (11,13), (12,14), (15,17), (16,18) with rigid connections <5,8>, <6,7>, <13,16>, <14,15>, elastic connections <1,1'> or <0,1> for active and passive pantographs and passive connections between the nodes <1,3>, <2,4>, <5,6>, <9,11>, <10,12>, <13,14>, <17,e>, <18,19>, <e,19> complemented by the connections <0,1> or <1,2> for active and passive pantographs. Active pantograph also contains a rigid link (1',2). Such presentation allows us to describe the elastic properties of pantographs by the following matrix equation

Table 1 Components of the MSA-based model of NAVARO II manipulator and its legs

Mechanical structure	Structural components				
	Passive joints	***Elastic joints***	***Rigid joint***	***Elastic links***	***Rigid links***
Active pantograph	<0,1>, <1,3>, <2,4>, <5,6>, <9,11>, <10,12>, <13,14>, <17,e>, <18,19>, <e,19>	<1,1'>	<5,8>, <6,7>, <13,16>, <14,15>	(3,5), (4,6), (7,9), (8,10), (11,13), (12,14), (15,17), (16,18)	(1',2)
Passive pantograph	<1,2>, <1,3>, <2,4>, <5,6>, <9,11>, <10,12>, <13,14>, <17,e>, <18,19>, <e,19>	<0,1>	<5,8>, <6,7>, <13,16>, <14,15>	(3,5), (4,6), (7,9), (8,10), (11,13), (12,14), (15,17), (16,18)	
Entire manipulator	<2a,3a>, <2b,3b>, <2c,3c>		<0a,1a>, <0b,1b>, <0c,1c>	(1a,2a), (1b,2b), (1c,2c), (3a,ep), (3b,ep), (3c,ep)	

$$\left[-\mathbf{I}_{96\times 96} \quad \mathbf{K}_{leg}\right]_{96\times 192}\cdot\begin{bmatrix}\mathbf{W}_{agr}\\ \Delta\mathbf{t}_{agr}\end{bmatrix}_{192\times 1}=\mathbf{0}_{96\times 1} \tag{23}$$

where $\Delta\mathbf{t}_{agr}$ and $\mathbf{W}_{agr}$ are the aggregated displacement and wrenches defined at the nodes from 3 to 18, $\mathbf{K}_{leg}$ aggregates stiffness matrices of links (3,5), (4,6), (7,9), (8,10), (11,13), (12,14), (15,17), (16,18) presented in the form (1) into a single matrix of a size 96×96 allowing to describe the manipulator leg elasticity.

For the considered manipulator, the MSA based model includes three types of passive joints and two types of elastic joints with passive directions around z and y-axis and translational joint in z directions, which are described by the following matrices

$$\mathbf{\Lambda}^{r}_{z^*}=\begin{bmatrix}1&0&0&0&0&0\\0&1&0&0&0&0\\0&0&1&0&0&0\\0&0&0&1&0&0\\0&0&0&0&1&0\end{bmatrix};\quad \begin{matrix}\mathbf{\Lambda}^{p}_{z^*}=\begin{bmatrix}0&0&0&0&0&1\end{bmatrix}\\ \mathbf{\Lambda}^{e}_{z^*}=\begin{bmatrix}0&0&0&0&0&1\end{bmatrix}\end{matrix} \tag{24}$$

$$\mathbf{\Lambda}^{r}_{yi^*}=\begin{bmatrix}1&0&0&0&0&0\\0&1&0&0&0&0\\0&0&1&0&0&0\\0&0&0&\cos\theta_i&0&\sin\theta_i\\0&0&0&-\sin\theta_i&0&\cos\theta_i\end{bmatrix};\quad \mathbf{\Lambda}^{p}_{y^*}=\begin{bmatrix}0&0&0&0&1&0\end{bmatrix} \tag{25}$$

$$\mathbf{\Lambda}^{r}_{t^*}=\begin{bmatrix}1&0&0&0&0&0\\0&1&0&0&0&0\\0&0&0&1&0&0\\0&0&0&0&1&0\\0&0&0&0&0&1\end{bmatrix};\quad \mathbf{\Lambda}^{p}_{t^*}=\begin{bmatrix}0&0&1&0&0&0\end{bmatrix} \tag{26}$$

where the matrix $\mathbf{\Lambda}^{r}_{yi^*}$ depends on the orientation of the ith leg of the manipulator and are different for all chains in non-symmetrical configurations. Using this notation, the constraints imposed by the passive joints <1,3>, <2,4>, <5,6>, <9,11>, <10,12>, <13,14>, <17,e>, <18,19> can be presented as

$$\begin{bmatrix}0&0&\mathbf{\Lambda}^{r}_{yi^*}&-\mathbf{\Lambda}^{r}_{yi^*}\\ \mathbf{\Lambda}^{r}_{yi^*}&\mathbf{\Lambda}^{r}_{yi^*}&0&0\\ \mathbf{\Lambda}^{p}_{y^*}&0&0&0\\0&\mathbf{\Lambda}^{p}_{r^*}&0&0\end{bmatrix}_{12\times 24}\cdot\begin{bmatrix}\mathbf{W}_i\\ \mathbf{W}_j\\ \Delta\mathbf{t}_i\\ \Delta\mathbf{t}_j\end{bmatrix}=\mathbf{0}_{12\times 1} \tag{27}$$

For passive pantograph it is required to consider additionally passive joint constraints for <1,2>, <e,19> while for active parallelogram only for joints <e,19>, i.e.

$$\begin{bmatrix}0&0&\mathbf{\Lambda}^{r}_{t^*}&-\mathbf{\Lambda}^{r}_{t^*}\\ \mathbf{\Lambda}^{r}_{t^*}&\mathbf{\Lambda}^{r}_{t^*}&0&0\\ \mathbf{\Lambda}^{p}_{t^*}&0&0&0\\0&\mathbf{\Lambda}^{p}_{t^*}&0&0\end{bmatrix}_{12\times 24}\cdot\begin{bmatrix}\mathbf{W}_i\\ \mathbf{W}_j\\ \Delta\mathbf{t}_i\\ \Delta\mathbf{t}_j\end{bmatrix}=\mathbf{0}_{12\times 1} \tag{28}$$

For an active parallelogram, the passive joint constraint for <0,1> is described as follows

$$\begin{bmatrix}0&0&\mathbf{\Lambda}^{r}_{z^*}&-\mathbf{\Lambda}^{r}_{z^*}\\ \mathbf{\Lambda}^{r}_{z^*}&\mathbf{\Lambda}^{r}_{z^*}&0&0\\ \mathbf{\Lambda}^{p}_{z^*}&0&0&0\\0&\mathbf{\Lambda}^{p}_{z^*}&0&0\end{bmatrix}_{12\times 24}\cdot\begin{bmatrix}\mathbf{W}_i\\ \mathbf{W}_j\\ \Delta\mathbf{t}_i\\ \Delta\mathbf{t}_j\end{bmatrix}=\mathbf{0}_{12\times 1} \tag{29}$$

Additionally for active pantograph it is required to take into account rigidity constraints (3) and (5) for the link (1',2), where vector $\mathbf{d}_i=[0,0,2l\sin\beta_i]^T$.

Translation elastic joint <1,1'> for active pantograph adding in the system the following equations

$$\left[\begin{array}{cc:cc}\mathbf{\Lambda}^{r}_{t^*}&-\mathbf{\Lambda}^{r}_{t^*}&\mathbf{0}_{5\times 6}&\mathbf{0}_{5\times 6}\\ \mathbf{0}_{6\times 6}&\mathbf{0}_{6\times 6}&\mathbf{I}_{6\times 6}&\mathbf{I}_{6\times 6}\\ \mathbf{K}^{e}_{t}\mathbf{\Lambda}^{e}_{t^*}&-\mathbf{K}^{e}_{t}\mathbf{\Lambda}^{e}_{t^*}&\mathbf{\Lambda}^{e}_{t^*}&\mathbf{0}_{1\times 6}\end{array}\right]\left[\begin{array}{c}\Delta\mathbf{t}_i\\ \Delta\mathbf{t}_j\\ \hdashline \mathbf{W}_i\\ \mathbf{W}_j\end{array}\right]=\left[\begin{array}{c}\mathbf{0}_{5\times 1}\\ \mathbf{0}_{6\times 1}\\ \mathbf{0}_{1\times 1}\end{array}\right] \tag{30}$$

where the coefficient $\mathbf{K}^{e}_{t}$ defines translation joint stiffness. Similarly, for passive pantograph rotation elastic join <0,1> adding in the system the following equations

$$\left[\begin{array}{cc:cc}\mathbf{\Lambda}^{r}_{z^*}&-\mathbf{\Lambda}^{r}_{z^*}&\mathbf{0}_{5\times 6}&\mathbf{0}_{5\times 6}\\ \mathbf{0}_{6\times 6}&\mathbf{0}_{6\times 6}&\mathbf{I}_{6\times 6}&\mathbf{I}_{6\times 6}\\ \mathbf{K}^{e}_{\varphi}\mathbf{\Lambda}^{e}_{z^*}&-\mathbf{K}^{e}_{\varphi}\mathbf{\Lambda}^{e}_{z^*}&\mathbf{\Lambda}^{e}_{z^*}&\mathbf{0}_{1\times 6}\end{array}\right]\left[\begin{array}{c}\Delta\mathbf{t}_i\\ \Delta\mathbf{t}_j\\ \hdashline \mathbf{W}_i\\ \mathbf{W}_j\end{array}\right]=\left[\begin{array}{c}\mathbf{0}_{5\times 1}\\ \mathbf{0}_{6\times 1}\\ \mathbf{0}_{1\times 1}\end{array}\right] \tag{31}$$

where the coefficient $\mathbf{K}^{e}_{\varphi}$ defines rotation joint stiffness.

For both pantographs, it is required to take into account that pantograph contains only 4 component by introducing rigid joint constraints via equations (6) and (7) for the joints <5,8>, <6,7>, <13,16>, <14,15>. Due to particularities of the above-described assumptions, for both active and passive pantographs, boundary constraints are introduced in the system for the node <0> via rigid constraint (11) and external force introduces via eq.(14) for the node <e>. Combining all above-mentioned equations it is possible to write stiffness

model for active and passive pantographs in the form (15), where for passive pantograph the size of the main matrix has the size of 252×288 and for active pantograph has the size of 264×294. It is obvious that the system of equation is over-constrained, so to find the desired Cartesian stiffness matrix using expression(17) pseudo inversion should be used.

4.2. MSA models of NAVARO II parallel manipulator

Using the stiffness model of the transmission system, it is possible to obtain the model of the entire manipulator can be presented as a non-rigid mobile platform connected via passive joints to equivalent models of pantograph-type transmissions fixed at another end. In this case to describe elasticity of mobile platform one can use eq. (2) and for legs flexibility reduced form of eq. (1), where the first node is eliminated because of the rigid connection to the base. The latter allows us to use only 6×6 stiffness matrices to describe elasticities of the pantograph-type transmission system. Passive joints for the connections <2a,3a>, <2b,3b>, <2c,3c> describes using expression (29). External loading applied to the platform end-effector <ep> is introduced via eq. (14) Combining all above-mentioned equations into a single system of equations one can get a system of order 84 (with the matrix of the size 84×84) in the form (15) and (16) that can be solved with respect to the reaction of the end effector node <ep> on the external wrench applied to it using eq. (17). This stiffness matrix can be computed for any reachable end-effector location and used for stiffness analysis of manipulator behavior within its workspace.

7. CONCLUSIONS

This paper deals with the stiffness modeling of a new type of parallel manipulator NAVARO II with a pantograph-type transmission system. The desired models were obtained using the enhanced matrix structural analysis (MSA) approach that is able to analyze the under-actuated and over-constrained structures with numerous passive joints. The MSA technique was applied to active and passive pantograph-type mechanisms for which the stiffness models operate with the matrices of sizes 252×288 and 264×294 respectively. MSA-based model for the entire manipulator with equivalent models for the pantograph-type transmission legs stiffness models operates with the matrix of sizes 84×84. These models will be used for manipulator parametric optimization and stiffness analysis of NAVARO II manipulator with different types of actuation modes.

ACKNOWLEDGMENTS

The work presented in this paper was supported by the grant of the Russian Science Foundation №17-19-01740.

REFERENCES

Alici, G. and Shirinzadeh, B. (2005) 'Enhanced stiffness modeling, identification and characterization for robot manipulators', *Robotics, IEEE Transactions on,* 21(4), pp. 554-564.

Chablat, D. and Rolland, L. (2018) 'NaVARo II: A New Parallel Robot With Eight Actuation Modes', V05AT07A043.

Deblaise, D., Hernot, X. and Maurine, P. 'A systematic analytical method for PKM stiffness matrix calculation'. *IEEE International Conference on Robotics and Automation (ICRA 2006)*: IEEE, 4213-4219.

Gosselin, C. (1990) 'Stiffness mapping for parallel manipulators', *Robotics and Automation, IEEE Transactions on,* 6(3), pp. 377-382.

Gosselin, C. and Zhang, D. (2002) 'Stiffness analysis of parallel mechanisms using a lumped model', *International Journal of Robotics and Automation,* 17(1), pp. 17-27.

Klimchik, A., Ambiehl, A., Garnier, S., Furet, B. and Pashkevich, A. (2017a) 'Comparison study of industrial robots for high-speed machining', in Zhang, D. & Wei, B. (eds.) *Mechatronics and Robotics Engineering for Advanced and Intelligent Manufacturing*: Springer International Publishing.

Klimchik, A., Ambiehl, A., Garnier, S., Furet, B. and Pashkevich, A. (2017b) 'Efficiency evaluation of robots in machining applications using industrial performance measure', *Robotics and Computer-Integrated Manufacturing,* 48, pp. 12-29.

Klimchik, A., Chablat, D. and Pashkevich, A. 'Advancement of MSA-Technique for Stiffness Modeling of Serial and Parallel Robotic Manipulators'. *ROMANSY 22 – Robot Design, Dynamics and Control*. Cham: Springer International Publishing, 355-362.

Klimchik, A. and Pashkevich, A. (2017) 'Serial vs. quasi-serial manipulators: Comparison analysis of elasto-static behaviors', *Mechanism and Machine Theory,* 107, pp. 46-70.

Klimchik, A., Pashkevich, A., Caro, S. and Chablat, D. (2012) 'Stiffness matrix of manipulators with passive joints: computational aspects', *Robotics, IEEE Transactions on,* 28(4), pp. 955-958.

Klimchik, A., Pashkevich, A. and Chablat, D. (2013) 'CAD-based approach for identification of elasto-static parameters of robotic manipulators', *Finite Elements in Analysis and Design,* 75, pp. 19-30.

Klimchik, A., Pashkevich, A. and Chablat, D. 'MSA Technique for Stiffness Modeling of Manipulators with Complex and Hybrid Structures'. *12TH IFAC SYMPOSIUM ON ROBOT CONTROL - SYROCO 2018*, Budapest, Hungary.

Klimchik, A., Pashkevich, A. and Chablat, D. (2019b) 'Fundamentals of manipulator stiffness modeling using matrix structural analysis', *Mechanism and Machine Theory,* 133, pp. 365-394.

Marie, S., Courteille, E. and Maurine, P. (2013) 'Elasto-geometrical modeling and calibration of robot manipulators: Application to machining and forming applications', *Mechanism and Machine Theory,* 69, pp. 13-43.

Nagai, K. and Liu, Z. 'A systematic approach to stiffness analysis of parallel mechanisms'. *Robotics and Automation, 2008. ICRA 2008. IEEE International Conference on*: IEEE, 1543-1548.

Pashkevich, A., Klimchik, A., Caro, S. and Chablat, D. 'Cartesian stiffness matrix of manipulators with passive joints: Analytical approach'. *Intelligent Robots and Systems (IROS), 2011 IEEE/RSJ International Conference on*, 4034-4041.

Pashkevich, A., Klimchik, A. and Chablat, D. (2011b) 'Enhanced stiffness modeling of manipulators with passive joints', *Mechanism and machine theory,* 46(5), pp. 662-679.

Quennouelle, C. and Gosselin, C. m. 'Instantaneous kinemato-static model of planar compliant parallel mechanisms'. *ASME 2008 International Design Engineering Technical Conferences and Computers and Information in Engineering Conference*: American Society of Mechanical Engineers, 163-173.

Wang, Y. Y., Huang, T., Zhao, X. M., Mei, J. P., Chetwynd, D. G. and Hu, S. J. 'Finite Element Analysis and Comparison of Two Hybrid Robots-the Tricept and the TriVariant'. *Intelligent Robots and Systems, 2006 IEEE/RSJ International Conference on*, 9-15 Oct. 2006, 490-495.

Yan, S. J., Ong, S. K. and Nee, A. Y. C. (2016) 'Stiffness analysis of parallelogram-type parallel manipulators using a strain energy method', *Robotics and Computer-Integrated Manufacturing,* 37, pp. 13-22.